ELSEVIER

Chemical Geology 222 (2005) 183–199

CHEMICAL GEOLOGY
INCLUDING
ISOTOPE GEOSCIENCE

www.elsevier.com/locate/chemgeo

Sr isotope systematics of K-feldspars in plutonic rocks revealed by the Rb–Sr microdrilling technique

W. Siebel *, E. Reitter, T. Wenzel, U. Blaha

Institut für Geowissenschaften, Universität Tübingen, Wilhelmstraße 56, 72074 Tübingen, Germany

Received 26 October 2004; received in revised form 10 June 2005; accepted 29 June 2005

Abstract

$^{87}Sr/^{86}Sr$ isotope variation was studied in subareas of K-feldspar megacrysts from Late-Palaeozoic granodiorite, diorite and syenite of the Bavarian Forest. Most samples were collected close to the Bavarian Pfahl shear zone and feldspars from these sites reveal remarkably constant initial $^{87}Sr/^{86}Sr$ isotope ratios. These ratios are similar to those of the bulk groundmass or feldspar crystals from the groundmass. Individual feldspar grains however, define isochron ages that are considerably younger (by ~15 to ~30 Ma) than the crystallisation age of the host rocks as defined by U–Pb and Pb–Pb zircon geochronology. The Rb–Sr feldspar data probably reflect diffusion controlled isotopic homogenisation under hydrous conditions between 290–310 Ma. A pink feldspar crystal from a hydrothermally altered syenite reveals comparatively large degree of isotopic variation, indicating local disturbance of the Rb–Sr system caused by hydrothermal alteration during Permian–Triassic Pfahl quartz precipitation. A diorite from the Fürstenstein pluton displays some isotopic scatter and slight differences in the initial $^{87}Sr/^{86}Sr$ ratios between the more radiogenic feldspar–megacryst and the less radiogenic bulk groundmass. This rock type was subsequently intruded by the Saldenburg granite and the more radiogenic $^{87}Sr/^{86}Sr$ isotope signature of the feldspar relative to the groundmass is interpreted as being consistent with the feldspar having exchanged with the fluids derived from the granite.

This study shows that K-feldspar crystals from slowly cooled plutonic rocks do not necessarily preserve their original Sr isotope composition. However, Sr isotope traverses through single crystals can give robust records of the mm-scale isotope system behaviour also in older plutonic rocks relevant for solving petrological or geochronological problems.

Keywords: Bavarian Forest; K-feldspar; Plutonic rock; Microdrilling; Pfahl zone; Sr-87/Sr-86

1. Introduction

Since the technical improvement of high precision analytical facilities, a number of studies attest to the growing interest in various microanalytical approaches (see Müller, 2003, for a review). Microsampling tech-

* Corresponding author. Tel.: +49 7071 29 74 991; fax: +49 7071 29 57 13.
E-mail address: wolfgang.siebel@uni-tuebingen.de (W. Siebel).

0009-2541/$ - see front matter © 2005 Elsevier B.V. All rights reserved.
doi:10.1016/j.chemgeo.2005.06.012

niques increase the spatial resolution and can provide important insights into single mineral composition that would not be revealed by whole-rock or bulk mineral analyses. In the field of radiogenic isotope geochemistry the microsampling technique, i.e., small-scale sampling of individual crystals has mainly been used for Sr isotope studies of feldspar minerals. Sr isotopic disequilibrium between crystals and bulk groundmass or within individual crystals has been found in a number of studies (Christensen and DePaolo, 1993; Christensen et al., 1995; Cox et al., 1996; Geist et al., 1988; Halama et al., 2002; Waight et al., 2000a,b) and was interpreted as evidence of contamination, magma mingling and mixing, or a xenochrystic origin of the feldspar. Throughout the last decade measurement of $^{87}Sr/^{86}Sr$ isotope profiles through feldspar-phenocrysts (termed crystal isotope stratigraphy, Davidson et al., 1998) helped to quantify the role of open system processes in pre-eruptive magmas, e.g., the assimilation of wall rock material (Feldstein et al., 1994), or the addition of recharge magmas (Davidson and Tepley, 1997; Davidson et al., 2001; Knesel et al., 1999). Such studies which have been mainly applied to members of the plagioclase series also helped to decode crystal growth rates and timescales of magma differentiation (Christensen and DePaolo, 1993; Davidson et al., 2001; Davies et al., 1994; Gagnevin et al., 2005). $^{87}Sr/^{86}Sr$ in situ isotope studies have recently also successfully been applied to other minerals with high Sr concentration such as clinopyroxene for mantle xenoliths (Schmidberger et al., 2003) and apatite and carbonate for carbonatites (Bizzarro et al., 2003).

Apart from a few studies (e.g., Halama et al., 2002; Waight et al., 2000b), little information exists about the spatial Rb–Sr isotope distribution within feldspars from old plutonic rocks. One reason for this is that age correction on the $^{87}Sr/^{86}Sr$ ratios is needed to account for the decay of ^{87}Rb and this influences the precision of analyses in particular for samples with high Rb/Sr ratios. In this study we test the Rb–Sr microsampling technique by applying it to K-feldspar crystals from Late-Palaeozoic plutonic rocks. Feldspars were probed from granodiorite, diorite and syenite and their exact formation process is controversially discussed i.e., as phenocrysts or products of metasomatic exchange. Three out of four sample localities are situated along the Bavarian Pfahl zone (Fig. 1). The rocks along this zone underwent a complex crystallisation and cooling history. One sample was taken from a diorite close to the contact of a granite intrusion and, in fact, this grain may represent a porphyroblast, derived from infiltrating fluids from the

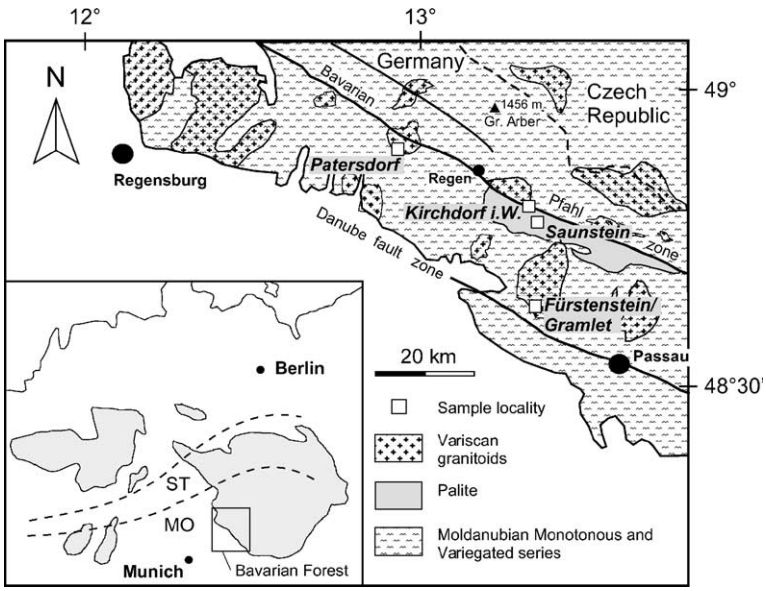

Fig. 1. Geological map of the Bavarian Forest (simplified from Christinas et al., 1991) showing the distribution of Late-Variscan magmatic rocks and location of samples (white squares) investigated in this study. Insert shows the location of the study area within the Bohemian Massif.

associated granite. However, isotopic contrasts between the granite-derived material and the host rock are required in order to judge whether such chemical flux has taken place. The specific aim of this study is to investigate if the isotope composition of K-feldspar megacrysts can provide information about their formation process.

2. K-feldspar-bearing samples

The sample localities are situated in the Bavarian Forest a portion of the south-western Bohemian Massif. Numerous Late-Variscan plutons are exposed within this basement complex which forms part of the Moldanubian domain (Fig. 1). Samples from four different localities were examined in detail and can be described as follows.

2.1. Saunstein-granodiorite

The Saunstein quarry is located close to the Bavarian Pfahl zone, a major Late-Variscan shear zone within the Bohemian Massif (Fig. 1). This locality hosts the best rock exposure within a granodioritic rock type which is also known as *palite* (Frentzel, 1911). Such rocks occur in a 5–7 km wide and approximately 50 km long stripe along the Pfahl zone (Fig. 1). The rocks are locally strongly deformed and possess a foliation of varying intensity. The most frequent rock type is a coarse-grained inequigranular, heterogeneous granodiorite that typically contains large megacrysts of white perthitic K-feldspar. The size of the feldspar megacrysts reaches up to 12 cm. The grains poikilitically enclose early-formed crystals of altered plagioclase. It was advocated by Troll (1967) and Steiner (1969, 1972) that this fabric, including the frequently observed fuzzy grain boundaries (Fig. 2a), may represent the metasomatic growth of K-feldspar. The K-rich metasomatic fluids were thought to be derived from Late-Variscan granites (Steiner, 1969, 1972). Microdrilling was performed on four different K-feldspar megacrysts. The groundmass of the investigated samples contains feldspar, quartz, biotite and amphibole with minor amounts of apatite, titanite, epidote and opaque minerals. Secondary calcite may also be found as a filling in narrow fissures of other minerals. Recently, Siebel et al. (2005) reported $^{207}Pb/^{206}Pb$ zircon evaporation ages of 334 ± 3 and 334.5 ± 1.1 Ma and concordant $^{238}U/^{206}Pb$ and $^{235}U/^{207}Pb$ ages between 328 and 341 Ma from two granodiorite samples. The samples were collected from rocks equivalent to those described here, ca. 10 and 20 km to the southeast of

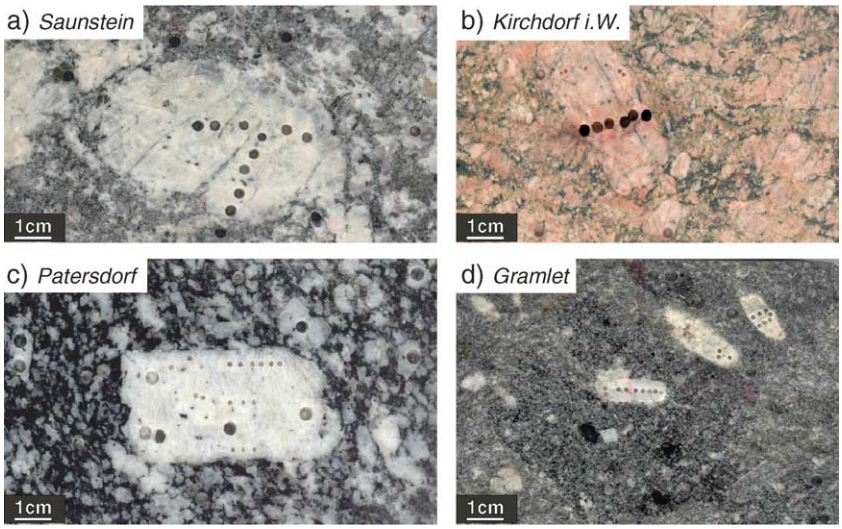

Fig. 2. Polished rock slabs; a) granodiorite, Saunstein quarry; b) syenite, hydrothermally altered with pink feldspar, Kirchdorf quarry; c) granodiorite from Patersdorf, Wildtier quarry; d) diorite from the Fürstenstein pluton, Gramlet quarry. Different sized holes represent sampling sites and are 2.0 and 0.5 mm in width.

the Saunstein quarry. Thus, an Ordovician formation age of the palite body as suggested by Christinas et al. (1991) on the basis of Rb–Sr whole-rock data can be ruled out and it is more likely that the Rb–Sr data represent a mixing line.

2.2. Kirchdorf im Wald-syenite

The Kirchdorf locality hosts a coarse-grained feldspar-rich fractured rock consisting principally of pink non-perthitic K-feldspar, with little or no quartz, and only small amounts of ferromagnesian minerals. The K-feldspar megacrysts lack visible grid-twinning and range from 2 to 10 cm in length. A 2 cm wide and 4 cm long K-feldspar megacryst was chosen for microdrilling (Fig. 2b). The groundmass mineral assemblage is similar to the Saunstein samples with the exception that amphibole was not observed in this rock type. Thin section analyses suggest that, following the solidification of the rock, subsequent deformation permitted introduced paleo-fluids to cause chemical modification. Given the close proximity to the Bavarian Pfahl zone (Fig. 1), this alteration might be an associated process of the Pfahl quartz mineralisation (see below). There are no age data available for the Kirchdorf syenite. The rock belongs to the same mappable rock unit as the Saunstein granodiorite. The change towards a syenitic composition could reflect secondary dissolution of quartz and associated K-metasomatism, and/or different stages of fractionation or magma mixing.

2.3. Patersdorf-granodiorite

The Wildtier quarry hosts the western outcrop of a previously unnamed intrusive body, hereafter informally referred to as the Patersdorf granite (Fig. 1). The locality is on the southwestern side of the Bavarian Pfahl zone. In this quarry the granite is in contact with two facies of biotite-granodiorite, a non-porphyritic, fine- to medium-grained variety and a coarse-grained variety with K-feldspar megacrysts. The latter was targeted in close contact to the Patersdorf granite. Typical feldspar grains of this variety are 2 to 6 cm in length. Microdrilling was carried out on a large K-feldspar megacryst, approximately 4 cm in length, embedded in a matrix of plagioclase, K-feldspar and quartz (Fig. 2c). Biotite is the sole mafic mineral in the investigated sample. The K-feldspars can display perthitic exsolution textures and wispy grid-twinning. The grains occasionally contain inclusions of plagioclase. U–Pb dating of zircons for granodiorites from the Wildtier quarry yields concordant $^{206}Pb/^{238}U$ and $^{206}Pb/^{238}U$ ages of 325 ± 3 and 326 ± 3 Ma, respectively (Siebel et al., in press). Zircon evaporation studies of two samples from the Patersdorf granite gave ages of 322 ± 5 (avg. $^{207}Pb/^{206}Pb$ age of three grains) and 323 ± 3 Ma (avg. $^{207}Pb/^{206}Pb$ age of four grains) (Siebel et al., in press).

2.4. Fürstenstein-diorite

The Fürstenstein intrusive complex is made up of five different granitic facies (Troll, 1964). Field and geochronological evidence suggest that these rocks were emplaced in a sequence of separate magma pulses over a long time interval (15–20 Ma, Chen and Siebel, 2004). Dioritic rocks represent the oldest intrusive unit and crop out intermittently in the southern part of the Fürstenstein pluton. The rocks are exposed in a number of quarries and were described in detail by Troll (1964). At the Gramlet quarry (Fig. 1), a massive diorite variety is intruded by the younger Saldenburg granite. The diorite was sampled a few meters away from the granite contact and contains megacrysts of white K-feldspar with diffuse boundaries, set in a dark matrix of plagioclase, biotite, quartz and rare amphibole (Fig. 2d). The feldspar crystals are twinned and display perthitic exsolutions. They differ from the K-feldspar megacrysts of the Pfahl zone granitoids described above by their smaller size. They are mostly ca. 1 cm in length and ellipsoidal in shape. The fact that the K-feldspar megacrysts occur isolated in a dioritic rock matrix (Fig. 2d) suggests that they are true porphyroblasts, which were formed by metasomatic processes during intrusion of the nearby Saldenburg granite. The diorites were dated at 330–334 Ma, whereas the Saldenburg granite yields an age of 312–318 Ma (U–Pb and Pb–Pb zircon data, Chen and Siebel, 2004).

3. Analytical techniques

Two different techniques are currently in use for Sr isotope analyses of individual crystals, namely the

microdrilling technique (see Davidson et al., 1998, for a review) and in situ laser ablation ICP-MS analysis (Christensen et al., 1995; Davidson et al., 2001; Waight et al., 2002; Ramos et al., 2004). Whereas the latter method requires greatly reduced sample preparation and analytical time, the more time-consuming microdrilling technique achieves higher precision of sub-ng Sr samples especially of those samples with high Rb/Sr ratios. In situ isotope analysis is difficult to realize for Rb-rich samples or older samples which have to be age-corrected for Rb-decay due to interfering isotopes or molecules that have masses that overlap those of Sr isotopes (Ramos et al., 2004). In the present study we have combined the microdrilling technique with scaled-down chromatographic and conventional isotope dilution Thermal Ionization Mass Spectrometry (ID-TIMS) techniques aspiring to obtain reasonably accurate initial $^{87}Sr/^{86}Sr$ ratios also for older (i.e., Variscan) rocks.

Feldspar samples were extracted from rock chips via microdrilling with diamond plated mandrels. Mandrel shank diameters were 2.0, 1.0 and 0.5 mm and drilling depth was generally less than 2 mm. The drilling produced a "plug" (generally 0.1–10 mg) that was checked for purity and inclusions under a binocular microscope and only samples with no visible dark, pinkish or opaque impurities were taken for isotope analyses. For comparison, material was also drilled from the bulk groundmass (i.e., matrix of fine-grained crystalline material around the K-feldspar megacrysts), and feldspars from the matrix. Thin sections were made from rock chips of the drilled crystals. Microprobe analyses were carried out on a JEOL JXA 8900RL electron microprobe using 15 kV accelerating voltage, 15 nA beam current, and a defocused beam 10 μm in diameter to prevent alkali loss. For Rb–Sr isotope analyses, the drilled material was dissolved in hot 52% HF for one day. Before digestion, a ^{87}Rb–^{84}Sr tracer solution was added to the sample. Digested samples were dried and re-dissolved in 6 N HCl, dried again and re-dissolved in 2.5 N HCl. Rb and Sr were isolated by conventional ion exchange chromatography on a set of quartz microcolumns with a 0.5 ml resin bed of Bio Rad AG 50W-X12, 200–400 mesh. All isotopic measurements were made on a Finnigan MAT 262 mass spectrometer in static cup configuration. Sr was loaded with a Ta–HF activator on pre-conditioned W-filaments and was measured in single-filament mode. Rb was loaded with ultra-pure H_2O on pre-conditioned Re-filaments and measurements were performed in a Re double filament configuration. The $^{87}Sr/^{86}Sr$ isotope ratios were normalised to $^{86}Sr/^{88}Sr=0.1194$. Repeated analysis of the Sr standard NBS 987 during the course of this study yielded a $^{87}Sr/^{86}Sr$ ratio of 0.710259 ± 12 (2σ SD, $n=28$). Total procedural blanks (chemistry and loading) were <200 pg for Sr. To assign realistic uncertainties to each initial $^{87}Sr/^{86}Sr$ ratio we have used an error equation made available by Prof. I. Wendt (written information — see Appendix). This equation includes an uncertainty of $\pm 1\%$ for the assumed crystallisation age. Based on 20 replicate analyses of the same sample powder within our lab, the external reproducibility (2σ, where σ is the standard deviation) is $\pm 1\%$ for the measured $^{87}Rb/^{86}Sr$ ratio, and of $\pm 0.02\%$ for the measured $^{87}Sr/^{86}Sr$ ratio and these values were taken for determining the best fit regression line to the data after Wendt (1986). The U–Pb analyses on zircon and titanite were carried out by standard isotope dilution methods as described in Chen and Siebel (2004) and U–Pb ages were calculated using the PbDat and Isoplot programs (Ludwig, 1993, 2003).

4. Compositional observations on K-feldspars from the Saunstein granodiorite

As mentioned above, it was argued that some of the feldspars from the Saunstein granodiorite body (i.e., palites) were formed by the infiltration of K-rich solutions (Troll, 1967; Steiner, 1969, 1972). Compositional properties of the feldspar crystals can address the question of whether the grains are magmatic or metasomatic in origin. The megacrysts contain abundant inclusions of altered plagioclase that are randomly distributed within the host. Microprobe analyses show that the feldspar megacrysts are predominantly composed of K-feldspar with near-identical composition between $Or_{93.7}Ab_{6.3}$ and $Or_{95.4}Ab_{4.6}$ (Table 1). The high Or content and the narrow compositional range are characteristic features of feldspars affected by metasomatism or solid-state re-equilibration (for examples, see Deer et al., 2001). By contrast, the K-feldspars formed by rapid cooling from a melt

Table 1
Microprobe analyses of feldspar megacrysts and plagioclase inclusion from the Saunstein granodiorite

	K-fsp[1a]	K-fsp[1a]	K-fsp[1a]	K-fsp[1a]	K-fsp[1b]	K-fsp[1b]	Plg[2]	Plg[2]	Plg[2]	Plg[2]
SiO_2 (wt.%)	64.63	64.70	63.44	64.56	64.50	64.60	60.82	60.95	60.62	60.80
Al_2O_3	18.17	18.08	18.75	18.25	18.20	18.01	24.57	24.35	24.55	24.47
FeO	0.05	0.05	–	0.04	0.12	0.05	0.22	0.24	0.19	0.17
CaO	–	–	–	–	–	–	6.91	6.71	6.86	6.81
Na_2O	0.54	0.58	0.56	0.64	0.54	0.47	7.47	7.66	7.63	7.56
K_2O	15.87	15.88	14.69	15.67	15.75	15.86	0.28	0.34	0.28	0.24
Total	100.23	100.08	100.83	100.11	100.15	99.62	100.51	100.40	100.27	100.23
Ba (ppm)	7800	5840	28,590	7230	6780	4880	–	–	–	–
Sr	830	1110	1620	1130	2320	690	1130	1080	1100	1470
X_{An}	0.0	0.0	0.0	0.0	0.0	0.0	33.3	32.0	32.7	32.8
X_{Ab}	5.3	5.6	5.9	6.3	5.3	4.6	65.2	66.2	65.8	65.9
X_{Or}	94.7	94.4	94.1	93.7	94.7	95.4	1.5	1.8	1.5	1.3

[1] Microprobe analyses from two different (a,b) feldspar megacrysts.
[2] Microprobe analyses from unaltered plagioclase inclusion within a K-feldspar megacryst.
– Below detection limit.

commonly display lower Or and higher Ab contents (ibid.). The K-feldspars from the investigated Saunstein granodiorite are often perthitic with regular lamellae of sodic plagioclase (Fig. 3a) and can show grid-twinning, characteristic of microcline. Electron microprobe analyses of unaltered feldspars demonstrate that the K-feldspar megacrysts from the Saunstein granodiorite display no discernible compositional zonation from core to rim. Amongst the analysed plagioclase inclusions only a few possess andesine composition around $An_{32–33}Ab_{65–66}Or_{1–2}$. The majority of the inclusions is altered into aggregates of sericite, albite and epidote/zoisite (Fig. 3b). This type of plagioclase alteration is also well developed along zones where the mineral is in contact with a K-feldspar grain (Fig. 3c). It argues for fluid mediated processes that accompanied low grade metamorphism or deformation of the Saunstein granodiorite. The fluid was probably also enriched in CO_2 and reaction between the fluid and Ca-rich plagioclase lead to the formation of secondary calcite and small calcite veins (see Section 2.1). In the presence of a CO_2-rich fluid phase K-feldspar is more resistant to alteration than plagioclase (Leichmann et al., 2003).

Amongst the trace elements Sr concentration is high and variable both in K-feldspar and plagioclase ranging from approximately 800 to more than 2300 ppm. Ba concentration is below detection limit (<200 ppm) in plagioclase but high Ba concentrations (5000 to 8000 ppm) were observed in the K-feldspars. Secondary K-feldspar with conspicuously high Ba (several wt.%) occurs in bright vein-like zones emanating from grain boundaries and extending into the "normal" K-feldspar grains (Fig. 3c, Table 1 column 3). It seems likely that movement of a fluid phase has led to precipitation of this secondary Ba-rich K-feldspar. Deformation and fracturing along the Pfahl zone may have aided fluid infiltration from the surrounding rocks during metamorphic or hydrothermal processes. Such fluids can easily penetrate along the grain boundaries, fracture zones or cracks. Thus, there is no doubt that metasomatic processes have modified the primary mineral assemblage of the Saunstein granodiorite. However, according to our observation, alteration and recrystallisation was mainly restricted to grain boundary zones and plagioclase inclusions. Concerning the question of K-feldspar megacryst formation, we think that a magmatic K-feldspar was locally replaced by Ba-rich feldspar and there is no clear evidence that this mineral was largely or completely formed by metasomatic replacement of other minerals. The high Or content of the "normal" K-feldspar may indicate slow cooling accompanied by solid-state re-equilibration.

5. Isotopic data

5.1. Rb–Sr K-feldspar data

From all rock types microdrilled samples were collected along traverses of large K-feldspar crystals.

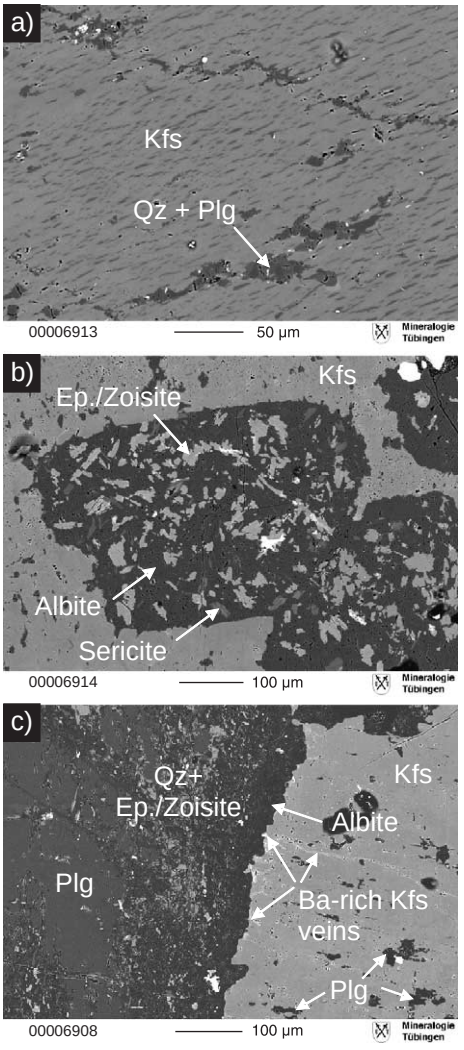

Fig. 3. Back-scattered electron images of feldspars from a Saunstein granodiorite; a) internal part of a large K-feldspar (perthitic) with uniformly distributed plagioclase lamellae (dark grey exsolved component) and inclusions of plagioclase–quartz aggregates; b) inclusions of plagioclase in K-feldspar in an advanced stage of replacement; the grain is decomposed into albite (dark grey), sericite or mica-like minerals (light grey) and zoisite/epidote (white); c) grain boundary alteration zone in plagioclase (left side) at contact with K-feldspar (right side). Plagioclase shows inner alteration zone of quartz and zoisite/epidote and outer zone of sodic plagioclase. The internal part still consists of primary plagioclase enriched in An component. Remnants of plagioclase (dark grey) also occur as isolated islands in the surrounding K-feldspar (light grey).

As evident from thin section petrography and microprobe analyses the analysed microsamples from the megacrysts do not represent pure K-feldspar analyses. Small inclusions of altered plagioclase frequently occur in the samples from the Saunstein and Kirchdorf samples.

For the *Saunstein* granodiorite Sr isotope data were acquired from four different grains (Table 2, Fig. 4). All grains are macroscopically similar to the grain shown in Fig. 2a. The feldspar microsamples contain high Sr concentration (avg. 860 ppm, isotope dilution data) and low $^{87}Rb/^{86}Sr$ ratios (0.6–1.1). Initial $^{87}Sr/^{86}Sr$ ratios were calculated for an age of 330 Ma (based on U–Pb and Pb–Pb data, see below). Sr isotopic compositions determined for an age of 290 Ma (avg. Rb–Sr feldspar age, see below) is shown for comparison in Fig. 4a. In all four grains the initial $^{87}Sr/^{86}Sr$ ratios overlap within analytical error and no discernible difference in the initial isotopic ratios between the K-feldspar megacrysts and the bulk groundmass around the K-feldspar megacrysts is observed. Christinas et al. (1991) analysed Sr isotopic composition of five whole-rock samples from the Saunstein quarry. Their data agree, within error, with the drill samples (Fig. 4b). When plotted in a Nicolaysen diagram (Fig. 5 a–d), the feldspar data define internal isochrons (using regression from Wendt, 1986) with ages of 289 ± 17 Ma (MSWD = 0.08), 292 ± 28 Ma (MSWD = 0.70), 310 ± 13 Ma (MSWD = 0.81) and 280 ± 29 Ma (MSWD = 1.48), significantly younger than the U–Pb and Pb–Pb zircon ages (Siebel et al., 2005; this study). The initial $^{87}Sr/^{86}Sr$ ratio of the four mineral isochrons is the same within analytical uncertainty (~0.707). When all K-feldspar data from the four megacrysts are combined an isochron age of 288 ± 8 Ma (MSWD = 0.93) with an initial $^{87}Sr/^{86}Sr$ ratio of 0.70707 ± 9 is obtained.

The investigated K-feldspar crystal from the *Kirchdorf* syenite is isotopically heterogeneous with no systematic difference in composition from core to rim. Compared to the unaltered samples from the Saunstein quarry, the microsamples from Kirchdorf contain lower Sr and higher Rb concentration, and consequently higher $^{87}Rb/^{86}Sr$ ratios (Table 2). Variation in initial $^{87}Sr/^{86}Sr$ ratios is very pronounced (0.0039 $^{87}Sr/^{86}Sr$ units) for an age of 330 Ma (Fig. 4a). The data define an errorchron (MSWD = 11) at 292 ± 2 Ma with an initial $^{87}Sr/^{86}Sr$ ratio of 0.70995 ± 10. For this age, the initial $^{87}Sr/^{86}Sr$ ratios are high (~0.7092–0.7108) and the variation is still very large (0.0016 $^{87}Sr/^{86}Sr$ units)

Table 2
Rb–Sr isotopic data of microsamples (Fsp = K-feldspar megacryst; Fsp matrix = feldspars from matrix; grdmass = bulk groundmass)

Sample/fraction	Weight (mg)	Rb (ppm)	Sr (ppm)	$^{87}Rb/^{86}Sr$	$^{87}Sr/^{86}Sr \pm 2\sigma_m$	$^{87}Sr/^{86}Sr_{init}$ [a]
Saunstein granodiorite						
Fsp 1.1	2.7	256	824	0.898	0.710744 ± 8	0.70647 ± 15
Fsp 1.2	4.4	254	1053	0.697	0.709892 ± 9	0.70658 ± 15
Fsp 1.3	6.6	283	782	1.047	0.711354 ± 10	0.70638 ± 16
Fsp 1.4	4.8	230	963	0.691	0.709909 ± 10	0.70662 ± 15
Fsp 2.1	4.0	232	815	0.823	0.710391 ± 10	0.70648 ± 15
Fsp 2.2	3.8	226	629	1.039	0.711316 ± 10	0.70638 ± 16
Fsp 2.3	3.0	227	791	0.832	0.710493 ± 10	0.70654 ± 15
Fsp 2.4	7.1	212	733	0.838	0.710555 ± 10	0.70657 ± 15
Fsp 2.5	3.6	249	769	0.937	0.710996 ± 9	0.70654 ± 16
Fsp 3.1	6.7	207	876	0.682	0.709772 ± 10	0.70653 ± 15
Fsp 3.2	6.5	259	787	0.950	0.710912 ± 10	0.70639 ± 16
Fsp 3.3[b]	4.3	241	823	0.848	0.710894 ± 9	0.70686 ± 15
Fsp 3.4	5.0	242	640	1.094	0.711496 ± 10	0.70630 ± 16
Fsp 3.5	8.0	205	775	0.764	0.710105 ± 10	0.70647 ± 15
Fsp 3.6	0.2	226	584	1.117	0.711757 ± 11	0.70645 ± 16
Fsp 4.1	5.3	242	1169	0.600	0.709662 ± 9	0.70681 ± 15
Fsp 4.2	10.2	273	1016	0.778	0.710323 ± 10	0.70662 ± 15
Fsp 4.3	15.6	259	988	0.760	0.710148 ± 10	0.70654 ± 15
Fsp 4.4	7.9	196	950	0.596	0.709485 ± 10	0.70665 ± 15
Fsp 4.5	22.6	236	948	0.719	0.710121 ± 10	0.70670 ± 15
Fsp matrix 1.1	5.6	234	716	0.944	0.711026 ± 10	0.70654 ± 16
Fsp matrix 3.1	7.3	291	718	1.175	0.711888 ± 9	0.70630 ± 16
Fsp matrix 4.1	19.8	302	693	1.262	0.712468 ± 10	0.70647 ± 17
Fsp matrix 4.2	23.1	155	574	0.780	0.710326 ± 10	0.70662 ± 15
Kirchdorf i.W. granite						
Fsp 5.1	9.2	303	198	4.433	0.729258 ± 10	0.70818 ± 33
Fsp 5.2	5.5	271	157	5.019	0.730980 ± 10	0.70712 ± 37
Fsp 5.3	3.3	353	167	6.128	0.735066 ± 10	0.70593 ± 44
Fsp 5.4	5.7	368	247	4.315	0.727877 ± 10	0.70736 ± 32
Fsp 5.5	4.8	367	224	4.758	0.729756 ± 10	0.70714 ± 35
Fsp 5.6	2.6	181	131	4.015	0.726331 ± 9	0.70725 ± 31
Fsp 5.7	2.1	268	160	4.865	0.729969 ± 8	0.70684 ± 36
Fsp 5.8	4.4	33	94	1.029	0.714098 ± 10	0.70921 ± 16
Fsp 5.9	3.1	387	157	7.144	0.738905 ± 10	0.70494 ± 50
Fsp 5.10	0.3	259	201	3.737	0.725472 ± 10	0.70771 ± 29
Fsp 5.11	0.3	450	313	4.170	0.727193 ± 12	0.70737 ± 32
Fsp 5.12	0.2	185	117	4.579	0.729348 ± 12	0.70758 ± 34
Patersdorf granodiorite						
Fsp 1.1	0.5	275	448	1.778	0.716804 ± 10	0.70858 ± 18
Fsp 1.2	0.7	245	583	1.217	0.714188 ± 9	0.70856 ± 16
Fsp 1.3	0.4	224	1003	0.646	0.711703 ± 7	0.70871 ± 15
Fsp 1.4	0.4	252	446	1.636	0.716114 ± 9	0.70855 ± 18
Fsp 1.5	0.4	226	514	1.273	0.714549 ± 10	0.70866 ± 17
Fsp 1.6	0.4	159	625	0.736	0.712228 ± 10	0.70882 ± 15
Fsp 1.7	0.5	245	432	1.642	0.716018 ± 9	0.70842 ± 18
Fsp 1.8	0.4	270	448	1.745	0.716629 ± 10	0.70856 ± 18
Fsp 1.9	2.3	246	525	1.357	0.714649 ± 10	0.70837 ± 17
Fsp 1.10	2.1	242	496	1.413	0.714996 ± 10	0.70846 ± 17
Fsp 1.11	3.6	252	528	1.382	0.714844 ± 7	0.70845 ± 17
Fsp matrix 1.1	1.5	44	494	0.258	0.709907 ± 9	0.70871 ± 14

Table 2 (*continued*)

Sample/fraction	Weight (mg)	Rb (ppm)	Sr (ppm)	$^{87}Rb/^{86}Sr$	$^{87}Sr/^{86}Sr \pm 2\sigma_m$	$^{87}Sr/^{86}Sr_{init}$ [a]
Patersdorf granodiorite						
Fsp matrix 1.2	3.1	5	558	0.026	0.708805 ± 8	0.70869 ± 14
Fsp matrix 1.3	3.6	94	337	0.807	0.712227 ± 8	0.70849 ± 15
Grdmass 1.1	1.2	137	426	0.933	0.712829 ± 9	0.70851 ± 16
Grdmass 1.2	3.0	130	182	2.069	0.718124 ± 10	0.70855 ± 20
Fürstenstein diorite						
Fsp 1.1	0.1	219	296	2.144	0.716595 ± 11	0.70640 ± 20
Fsp 1.2	0.4	176	239	2.139	0.717261 ± 18	0.70709 ± 20
Fsp 1.3	0.4	206	379	1.569	0.714180 ± 10	0.70672 ± 18
Fsp 1.4	0.2	227	349	1.887	0.715925 ± 8	0.70695 ± 19
Fsp 1.5	0.4	218	288	2.191	0.717767 ± 10	0.70735 ± 21
Fsp 1.6	0.4	221	377	1.698	0.714612 ± 10	0.70654 ± 18
Fsp 1.7	0.5	70	486	0.417	0.709231 ± 8	0.70725 ± 14
Fsp 1.8	0.7	176	390	1.306	0.713434 ± 10	0.70722 ± 17
Grdmass 1.1	5.1	198	239	2.395	0.717538 ± 11	0.70615 ± 22
Grdmass 1.2	5.9	216	257	2.438	0.716235 ± 9	0.70464 ± 22
Grdmass 1.3	6.3	187	266	2.036	0.715753 ± 10	0.70608 ± 20
Grdmass 1.4	0.5	131	275	1.379	0.713426 ± 10	0.70687 ± 17
Grdmass 1.5	0.5	145	223	1.883	0.715513 ± 14	0.70656 ± 19
Grdmass 1.6	0.9	128	265	1.398	0.713464 ± 10	0.70682 ± 17
Grdmass 1.7	1.0	184	262	2.034	0.715894 ± 9	0.70623 ± 20
Grdmass 1.8	0.7	134	295	1.315	0.713203 ± 10	0.70695 ± 17

First sample no. = no. of grain; second no. = number of analyses within individual grain. Data points shown in relative core-to-rim position for each grain (comp. Fig. 4).

[a] Initial $^{87}Sr/^{86}Sr$ ratios calculated for $T = 330$ Ma (Saunstein, Kirchdorf, Fürstenstein) and 325 Ma (Paters-dorf); uncertainty of this ratio was derived from the equation given in the Appendix.

[b] Analyses omitted from isochron calculation in Fig. 5.

compared to the samples from the Saunstein granodiorite (Fig. 4a).

The analysed K-feldspar megacryst from the *Patersdorf* granodiorite shows no variation in initial $^{87}Sr/^{86}Sr$ ratios, within analytical precision (less than 0.0004 $^{87}Sr/^{86}Sr$ units). The $^{87}Sr/^{86}Sr_{325\ Ma}$ ratios of the megacryst are identical, within error, to those of bulk groundmass and matrix feldspar (Fig. 4b). When plotted in a Nicolaysen diagram (Fig. 5e), the feldspars define an internal isochron with an age of 308 ± 5 Ma ($Sr_{init} = 0.70889 \pm 1$, MSWD = 1.92), significantly younger than the U–Pb zircon age of the rock (325 ± 2 Ma). Sr concentration lies generally between 400 and 600 ppm. The high Sr concentration of 1003 ppm and the low Rb/Sr ratio of one microsample from the megacryst (Fsp 1.3 in Table 2) can be explained by small inclusions of apatite. The Rb concentrations and the Rb/Sr ratios of the matrix feldspar are low compared to the K-feldspar megacryst. This could indicate a higher contribution of plagioclase within the matrix analyses. Fig. 4b also shows a $^{87}Sr/^{86}Sr$ whole-rock analysis of the granodiorite specimen from which the feldspar was investigated (data from Siebel et al., in press). This sample has a very similar isotopic signature as the microdrill samples implying that equilibrium was attained between the K-feldspar and the rest of the rock. Rb–Sr isotope ratios are also available for whole-rock samples from the Patersdorf granite (Siebel et al., in press). Compared to granodiorite the granite yields consistently less radiogenic $^{87}Sr/^{86}Sr$ ratios (0.7067–0.7071, Fig. 4b).

The K-feldspar megacryst from the *Fürstenstein diorite* yields a wide range in $^{87}Sr/^{86}Sr_{330\ Ma}$ ratios (0.0010 $^{87}Sr/^{86}Sr$ units). In a Nicolaysen diagram (Fig. 5f), the data scatter around a reference line of 320 ± 3 Ma (MSWD = 18) with an initial $^{87}Sr/^{86}Sr$ ratio of 0.70728 ± 8. The bulk groundmass adjacent to the feldspar megacryst yields a similar scatter (0.0008 $^{87}Sr/^{86}Sr$ units) and is displaced to slightly lower $^{87}Sr/^{86}Sr_{330\ Ma}$ ratios even when a sample with a remarkable low $^{87}Sr/^{86}Sr_{330\ Ma}$ ratio is excluded from the data set (Fig. 4b).

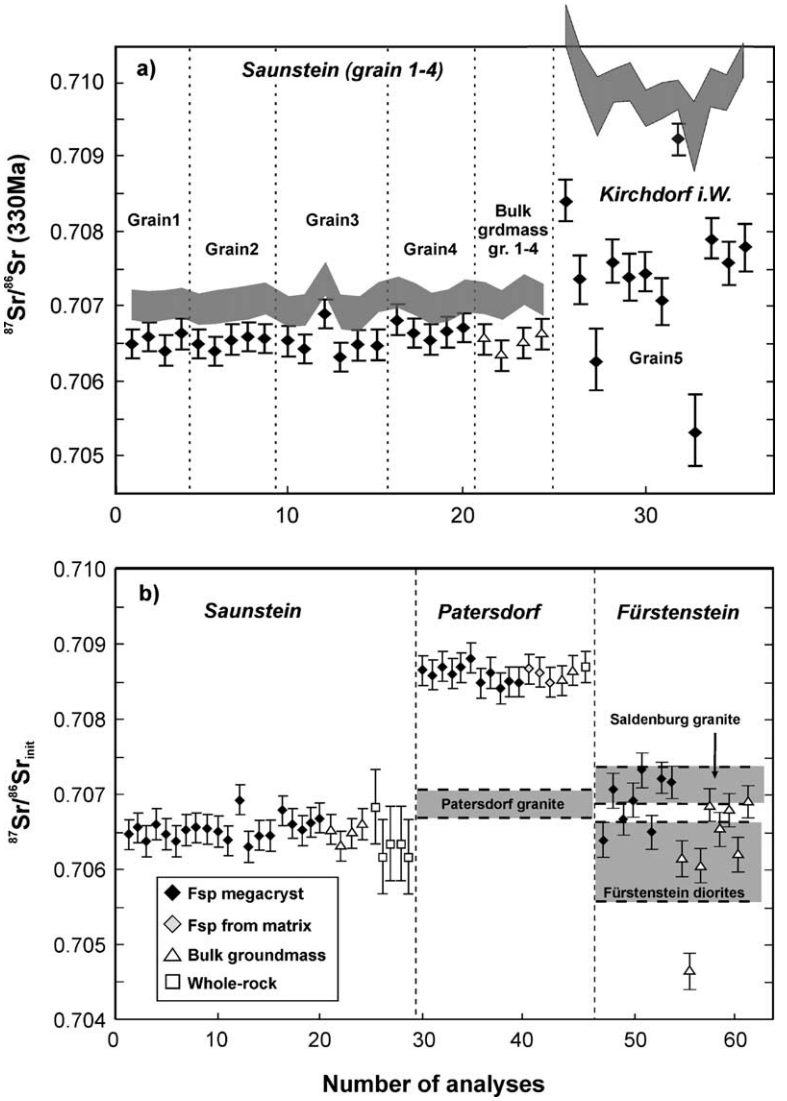

Fig. 4. $^{87}Sr/^{86}Sr$ isotope data of megacrysts (black diamonds) from granodiorites and diorites rocks of the Bavarian Forest. Data points are shown in relative core-to-rim position for individual crystals. All error bars are $\pm 2\sigma$ calculated according to the formula given in the Appendix. a) Four different megacrysts (grains 1–4) from unaltered granodiorite and one grain (grain 5) from an altered syenite sample with $^{87}Sr/^{86}Sr$ initial ratios at 330 Ma. Both samples are from the same igneous rock complex (*palites,* sensu Frentzel, 1911). Analytical errors of grain 5 are higher than those of grains 1–4 due to higher Rb/Sr ratios of this grain. The four open triangles represent bulk groundmass analyses. Gray area depicts range (2σ) of $^{87}Sr/^{86}Sr$ isotope ratios obtained for 290 Ma (close to avg. Rb–Sr feldspar age). b) Comparison of the initial $^{87}Sr/^{86}Sr$ isotopic compositions of feldspar crystals from Saunstein, Patersdorf and Fürstenstein. Isotope ratios calculated back to 330 Ma for Saunstein and Fürstenstein and 325 Ma for Patersdorf. Shaded diamonds represent feldspars from the matrix, open squares are $^{87}Sr/^{86}Sr$ whole-rock data from literature; data for Saunstein quarry from Christinas et al. (1991), for Patersdorf from Siebel et al. (in press). Shaded fields show the range of $^{87}Sr/^{86}Sr$ whole-rock ratios measured in the Patersdorf and Saldenburg granites and the Fürstenstein diorites (data from Chen and Siebel, 2004 and Siebel et al., in press).

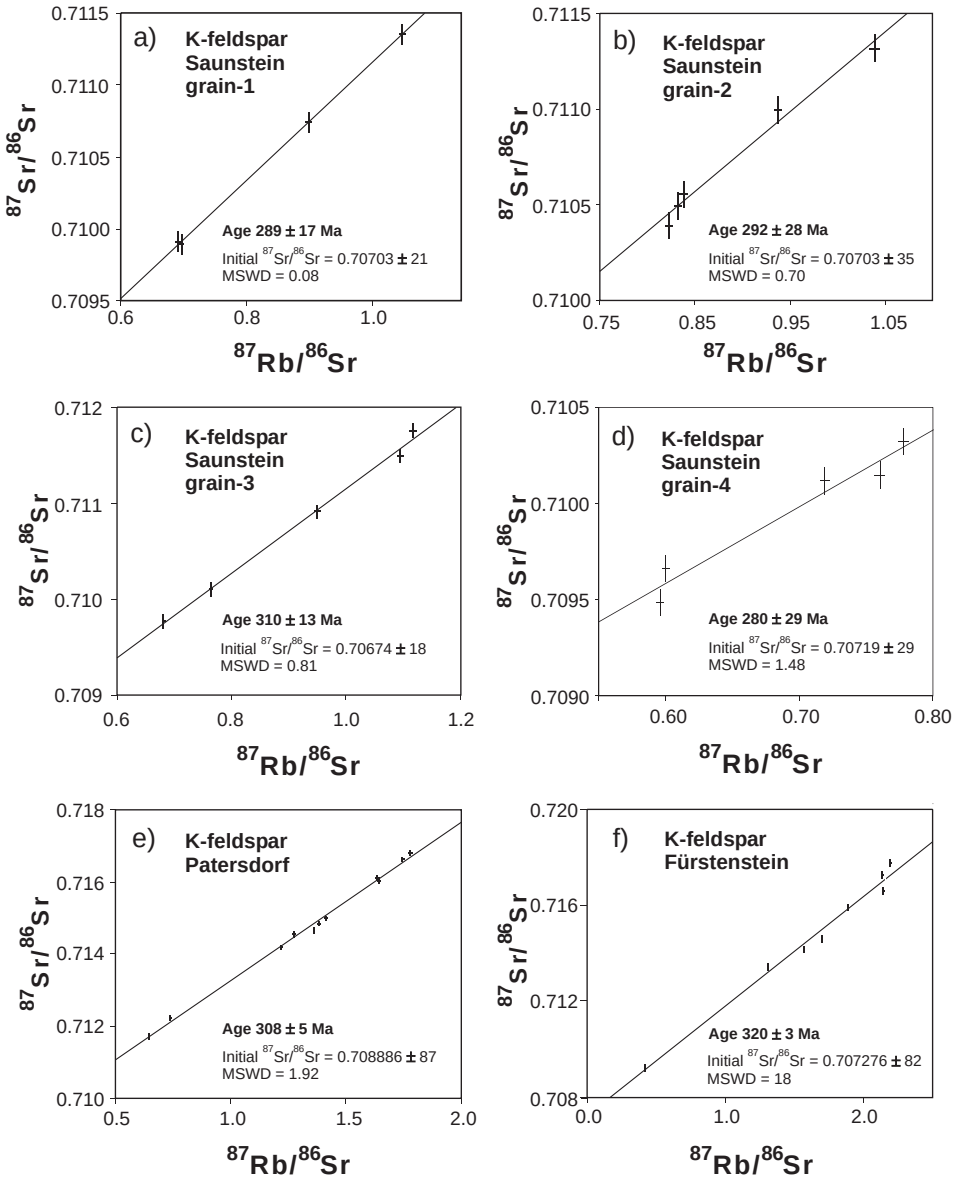

Fig. 5. $^{87}Sr/^{86}Sr$ vs. $^{87}Rb/^{86}Sr$ isotope diagrams for drilled portions of different feldspar megacrysts. a–d) different grains from the Saunstein granodiorite; data points in Fig. 4c were fitted disregarding analyses of Fsp 3.3 which appears to have incorporated some extra radiogenic Sr or suffered some degree of Rb loss (Table 2). e) Rb–Sr analyses from feldspar from the Patersdorf granodiorite, Wildtier quarry; f) Rb–Sr analyses from feldspar from the Fürstenstein diorite, Gramlet quarry. Note that the Fürstenstein data define an "errorchron". Regression line parameters were calculated after Wendt (1986). Uncertainties in ages and initial ratios are given at 95% confidence level.

5.2. U–Pb zircon and titanite data

In order to provide complementary information to the crystallisation and cooling history of the Saunstein granodiorite ID-TIMS U–Pb analyses on zircon and titanite was performed. Two non-abraded single zircon analyses from the Saunstein granodiorite yield concordant or near concordant $^{238}U/^{206}Pb$ and $^{235}U/^{207}Pb$ ages of 325 Ma (Table 3) with $^{207}Pb/^{206}Pb$ ages of 326 and 335 Ma. In a Concordia diagram (Fig. 6) these

Table 3
U and Pb isotopic composition for zircon and titanite grains from the Saunstein granodiorite

Sample/ Fraction[a]	Weight[b] (mg)	$^{206}Pb^{c}/^{204}Pb$	U[b] (ppm)	Pb[b] (ppm)	Th/U[d]	Isotopic ratios[e]			Calculated ages (Ma)		
						$^{206}Pb/^{238}U$	$^{207}Pb/^{235}Pb$	$^{207}Pb/^{206}Pb$	$^{206}Pb/^{238}U$	$^{207}Pb/^{235}U$	$^{207}Pb/^{206}U$
Zirc-p60-1	0.021	613	1619	92	0.86	0.05176 ± 45	0.3777 ± 35	0.05293 ± 14	325	325	326
Zirc-p60-2	0.048	4818	1463	74	0.42	0.05159 ± 29	0.3780 ± 21	0.05314 ± 5	324	326	335
Tit-396-1	0.041	44.9	92	20	4.3	0.04930 ± 47	0.3574 ± 103	0.05255 ± 137	310	310	310
Tit-396-2	0.070	34.7	92	27	4.1	0.05106 ± 69	0.3718 ± 204	0.05281 ± 266	321	321	321
Tit-396-3	0.071	44.2	61	15	6.1	0.05023 ± 48	0.3628 ± 134	0.05238 ± 183	316	314	302
Tit-396-4	0.078	48.0	99	21	4.5	0.05031 ± 43	0.3488 ± 155	0.05029 ± 209	316	304	208
Tit-396-5	0.113	27.9	83	39	7.5	0.05022 ± 35	0.3549 ± 195	0.05125 ± 266	316	308	252
Tit-396-6	0.113	64.0	146	21	2.4	0.04965 ± 168	0.3590 ± 133	0.05244 ± 69	312	311	305

[a] Data for zircon (zirc-p60) comprise non-abraded single grains; titanite grains (tit-396) were selected from different grain size fractions (1 and 2: 63–112 μm; 3 and 4: 112–200 μm; 5 and 6: 200–315 μm) and either single grains or populations consisting of 2–5 grains were analysed.
[b] Weight and concentration error better than 20%.
[c] Measured ratio corrected for mass discrimination and isotope tracer contribution.
[d] Th/U model ratio calculated from $^{208}Pb/^{206}Pb$ ratio and age of the sample.
[e] Corrected for blank Pb, U, and initial common Pb based on K-feldspar analyses of the same sample with $^{206}Pb/^{204}Pb = 18.17$, $^{207}Pb/^{204}Pb = 15.60$ and $^{208}Pb/^{204}Pb = 38.18$; errors are 2σm and refer to the last digits.

ages define the younger end of an age interval which extends up to 342 Ma when U–Pb data for nine non-abraded zircon analyses from two other granodiorite samples of this rock type are included (Siebel et al., 2005). The large scatter is not the result of measurement uncertainty alone, probably reflecting the effect of more than one age component as well as minor Pb loss. Considering these limitations, an age of 330 Ma is regarded as the minimum crystallisation time of the Saunstein granodiorite.

Titanites were separated from various size fractions (63–315 μm) from a Saunstein granodiorite and comprise, without exception, xenomorphic crystals. Compared to the zircon analyses all fractions are low in U and rich in common Pb (Table 3). In such a case the choice of initial Pb isotope composition has significant

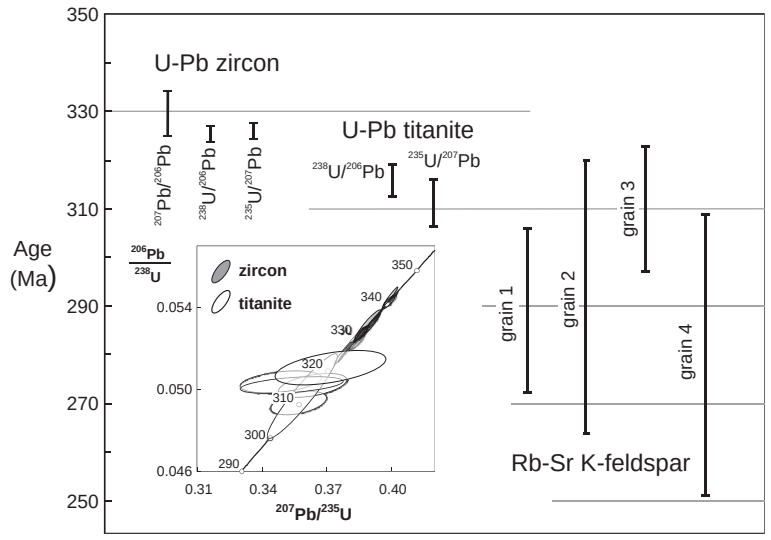

Fig. 6. Compilation of geochronological results from the Saunstein granodiorite including U–Pb and Pb–Pb zircon, U–Pb titanite and Rb–Sr feldspar analyses. The inset shows a U–Pb Concordia diagram of zircon and titanite analyses. The zircon data array shown in this diagram also includes analyses from two granodiorites from outside the Saunstein quarry (Siebel et al., 2005).

effect on the calculated ages. Therefore, the Pb isotope composition of a K-feldspar from the same sample was also analysed and used for common Pb correction (data shown in Table 3). Analysis of titanite resulted in six concordant analytical points which yielded a mean $^{206}Pb/^{238}U$ age of 315.4 ± 3.3 Ma and $^{207}Pb/^{235}U$ age of 311.0 ± 4.9 Ma. Isochrons derived from $^{238}U/^{206}Pb$ and $^{235}U/^{207}Pb$ ratios (not shown) define slopes that correspond to ages of 309 ± 9 Ma (MSWD = 5.3) and 305 ± 6 Ma (MSWD = 1.6), respectively. The good correspondence between the concordia ages and the isochron ages indicates that the common Pb correction used in calculating the concordia ages was appropriate. It is evident from the data that the U–Pb titanite ages are systematically younger by about 10–20 Ma than the U–Pb and Pb–Pb zircon ages (Fig. 6).

6. Discussion

As a basic result of this study, the K-feldspar megacrysts from the investigated granitoids record internal Rb–Sr isochron ages which are significantly younger than the crystallisation ages of the host rocks. K-feldspars from the Saunstein granodiorite and the Kirchdorf syenite were considered of metasomatic origin by previous workers (Troll, 1967; Steiner, 1969, 1972) and thus the feldspar data could reflect the metasomatic event. However, metasomatic feldspar growth seems not very likely to us based on our microprobe investigation. There is clear evidence that an aqueous fluid phase has reacted with the rock, and this fluid might have caused isotopic homogenisation long time after crystallisation. Alternatively, a slow cooling model has to be explored in order to see whether such a model can explain the radiometric data. In the following paragraphs these contrasting scenarios will be discussed more detailed.

The rocks in the Pfahl area probably experienced relative high temperature metamorphism over a period of time. Quartz microfabrics in mylonitic rocks from the Pfahl zone indicate that temperatures above 650 °C prevailed in this zone considerable time after the granitoid emplacement (Brandmayr et al., 1995). Thus, subsolidus evolution and recrystallisation could have permitted a post-magmatic Sr isotope exchange in the K-feldspars. In slowly cooled rocks Sr diffusion in K-feldspar might even take place at temperatures below 500 °C (Cherniak and Watson, 1992). If long lasting high temperatures (~500–700 °C) over protracted period of time (several million years) existed along the Bavarian Pfahl zone this could have caused Sr isotope exchange in K-feldspar.

Further criteria to assess the thermal history of the Saunstein sample appear when mineral data from this locality are compared in a closure temperature versus mineral age diagram (Fig. 7). Published Rb–Sr data for biotite from the Saunstein quarry (Christinas et al., 1991) is also shown in this diagram. For a single mineral the closure temperature, whose theoretical basis was examined by Dodson (1973), is variable and depends on cooling rate, grain size and shape. Nevertheless, some general observations can be made from Fig. 7. First, there appears a large hiatus between U–Pb zircon and U–Pb titanite data. This would imply slow cooling of the granodiorite of approximately 20 °C per Ma. Secondly, there is virtually no age difference between the U–Pb titanite and the Rb–Sr biotite system despite the higher closure

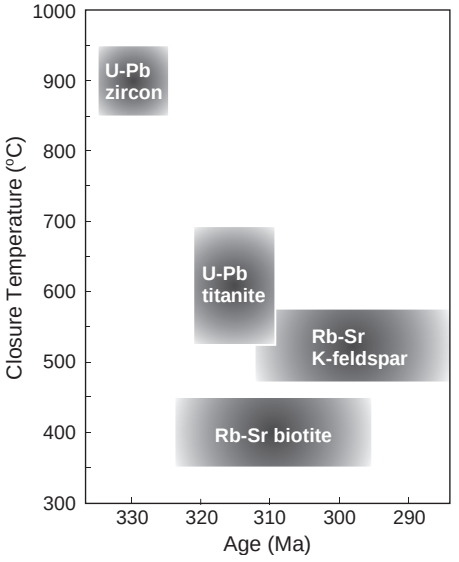

Fig. 7. Closure temperature versus mineral ages shown for minerals from the Saunstein quarry. Note that all age data are from the same locality. Rb–Sr age data for biotite are taken from Christinas et al. (1991). Closure temperatures are assumed to be 850–950 °C for zircon (Cherniak and Watson, 2000), 550–700 °C for titanite (Cherniak, 1993; Frost et al., 2000) and, assuming a cooling rate of 20°/Ma, as inferred from the zircon–titanite U–Pb data, 475–575 °C for K-feldspar (Giletti, 1991) and 350–450 °C for biotite (Giletti, 1991; Jenkin et al., 2001).

temperature assumed for titanite (Cherniak, 1993; Frost et al., 2000). The data also show that the biotites are shifted towards older ages compared to the K-feldspar ages, despite the higher closure temperature assumed for K-feldspar (Giletti, 1991; Cherniak and Watson, 1992). Given the fact that minerals with clearly different closure temperatures yield similar or even inconsistent age data, a slow cooling scenario — although it might have existed — is not a sufficient explanation for the Saunstein granodiorite.

Sr diffusion in feldspar (plagioclase and K-feldspar) may be an order of magnitude faster under hydrous conditions (Cherniak and Watson, 1992, 1994; Giletti, 1991; Giletti and Casserly, 1994). Under such circumstances there is an additional potential of down-temperature exchange of Sr isotopes amongst minerals (Jenkin et al., 1995) and the closure temperature estimates, predicted for dry conditions, are no longer applicable. During a post-magmatic hydrothermal or metasomatic event diffusional exchange within the feldspar megacrysts can occur in different ways. If fluid flow and metasomatic exchange is variable or spatially limited, isotopic disequilibrium would be expected and the Rb–Sr data should give "errorchrons" with high MSWD values and meaningless ages. However, if isotopic exchanges were pervasive, the Rb–Sr system would be reset completely and could produce meaningful age data, i.e., the age of the metasomatic or hydrothermal event. This might be a plausible model for the homogeneous Saunstein K-feldspars data. The Saunstein samples show overlap in the initial Sr isotopic ratios between K-feldspar megacrysts, bulk groundmass and feldspars from the matrix suggesting that resetting of the Rb–Sr system by isotopic re-distribution was a likely process at least on hand-specimen scale. In order to explain the low $^{87}Sr/^{86}Sr$ ratios of the feldspar isochrons (Fig. 5) a fluid phase with low Sr concentration and/or low $^{87}Sr/^{86}Sr$ ratios must be assumed for the Saunstein granodiorite.

The Saunstein, Kirchdorf and Patersdorf localities are located close to the Bavarian Pfahl shear zone (Fig. 1). The activity of a hydrothermal system in this zone is manifested by the formation of a huge quartz dike up to 150 km long and 100 m thick. The quartz forming event was dated by Rb–Sr analyses on pure quartz crystals at 247 ± 21 Ma (Horn et al., 1986). This passage of large quantities of aqueous fluids through the crust might affect the Rb–Sr system of the whole-rocks or minerals. However, the quartz forming fluids were substantially more radiogenic (0.7135, Horn et al., 1986) than most of our investigated feldspar samples and therefore, it is not very likely that this mineralisation event caused significant alteration. Only for the Kirchdorf locality, the samples have $^{87}Sr/^{86}Sr_{247\ Ma}$ ratios mainly between 0.712 and 0.714 and the isotopic disturbance observed in the pink feldspars from this sample might be attributed to hydrothermal alteration associated with the Pfahl quartz precipitation. The Kirchdorf locality lies closest to the centre of the Pfahl zone (Fig. 1). It appears from the hand specimen (Fig. 2b) that brittle deformation has created pathways for fluids in the rock, enabling Sr diffusivity even under hydrothermal low temperature conditions. The chemical features of the K-feldspars (low Sr, high Rb concentration, high Rb/Sr ratios) may imply a more advanced stage of magma fractionation of the Kirchdorf melt or, alternatively, it might be argued that Sr was lost and Rb was added during interaction with a high-$^{87}Sr/^{86}Sr$ fluid phase.

With respect to the feldspar analyses from the other localities along the Pfahl zone, it appears that the regressed data from Patersdorf have significantly higher initial $^{87}Sr/^{86}Sr$ ratios (~0.708–0.709) than the Saunstein data (~0.706–0.707) (Figs. 4 and 5). In case of a magmatic origin this would demonstrate the existence of two different parental melts; if the feldspars were homogenised by fluids this requires two relatively homogeneous fluids of quite distinct isotopic composition. New isotope data generated during a companion study (Siebel et al., in press) on whole-rock samples from the Patersdorf granite can help to further validate this point. There appears a marked difference in $^{87}Sr/^{86}Sr_{325\ Ma}$ ratio between the less radiogenic Patersdorf granite (0.7068 ± 2, 1σ, $n = 4$) and the more distinct radiogenic Patersdorf granodiorite (0.7088 ± 1, 1σ, $n = 16$) (Fig. 4b), from which the feldspar was analysed. This confirms a limited extent or total lack of Sr-isotopic re-equilibration between the granite and the granodiorite. It seems more likely, that both rocks were derived from different magma sources. Geochronological evidence from the micro-drill samples shows that isotope equilibration in the granodiorite feldspar grain was achieved at 308 ± 5

Ma (Fig. 5e). In this case we cannot rule out a slow cooling scenario given the lack of other mineral data. If the young K-feldspar age is a consequence of homogenisation by a fluid phase, this phase did obviously not homogenise the Sr budget between the granite and the granodiorite. Only a Sr poor fluid phase could have caused such an internal redistribution of the Sr on a single intrusion scale.

Preservation of isotopic disequilibrium is found in the diorite from the Fürstenstein pluton. The isotopic composition of this rock is interpreted as representing the products of chemical interaction with the Saldenburg granite. The introduction of volatiles released from this granite may be responsible for the isotopic disturbance. The Saldenburg granite has initial $^{87}Sr/^{86}Sr$ whole-rock ratios between 0.7069 and 0.7074 (Chen and Siebel, 2004). Such values correspond with those found in some of the K-feldspar megacrysts from the diorite (Fig. 4b). The diorites have slightly lower initial $^{87}Sr/^{86}Sr$ ratios between 0.7056 and 0.7067 (Chen and Siebel, 2004) which are at the lower range of values found in the investigated diorite. Thus, in this case study, transfer of volatiles from the granite into the diorite and partial re-crystallisation of feldspar in the diorite would explain the significant heterogeneity of the $^{87}Sr/^{86}Sr$ ratios as well as the fact that the feldspars are in isotopic disequilibrium with the whole-rock (Fig. 4b).

7. Conclusions

Sr isotope stratigraphy of K-feldspar megacrysts from plutonic rocks (granodiorite, diorite, syenite) with complicated history record post-magmatic subsolidus diffusive re-equilibration aided by a fluid phase (Saunstein) as well as isotopic disequilibrium features (Kirchdorf, Fürstenstein).

Individual K-feldspar crystals from the Saunstein granodiorite yield Permo–Carboniferous ages 15 to 30 Ma younger than the crystallisation age of the host rock. Further minerals from the same locality but with different closure temperatures (U–Pb titanite, Rb–Sr biotite) show similar young ages and thereby making it likely that these rocks achieved post-crystallisation isotopic homogenisation. The homogenisation of the Sr isotopic signature took place under thermo-metamorphic or hydrothermal conditions. The location of these rocks in the mineralized Bavarian Pfahl shear zone could have facilitated isotope exchange. Due to the lack of Sr isotopic contrast between K-feldspar megacrysts and the bulk groundmass around the megacrysts, a metasomatic formation of the K-feldspars from the Saunstein locality as claimed by Troll (1967) and Steiner (1969, 1972) cannot be substantiated by the isotope data set. Compositional characteristics and the presence of reaction textures, however, clearly indicate the infiltration of a fluid phase into this rock type.

K-feldspar crystals from the Patersdorf granodiorite show consistently more radiogenic Sr-isotope ratios compared to the adjacent granite. The growth of the megacrysts can therefore not be attributed to infiltration of volatile-rich residual fluids from the granite. Instead, it must be related to primary crystallisation as a phenocrysts phase from the granodioritic melt. Additional mineral data may permit to decide whether the young Rb–Sr feldspar ages found in the granodiorite result from slow cooling process or from late-stage fluid aided isotopic homogenisation.

Pink feldspars from the cataclastic Kirchdorf syenite, Bavarian Pfahl zone, show Sr isotopic disequilibrium. In this case, post-magmatic isotopic exchange with hydrothermal fluids of the Pfahl quartz system has caused the initial isotopic heterogeneity. Fractures and grain boundaries are inferred to have triggered the fluid migration. The brittle deformation texture of this rock suggests that isotope disturbance was controlled by crack formation during the late deformation of the K-feldspar-rich rock under retrograde (hydrous greenschist facies) conditions.

Isotopic heterogeneity found in the Fürstenstein diorite indicates that volatiles from the younger Saldenburg granite injected into the diorite thereby changing the isotope composition. This interaction took place at a relatively low temperature or over a short period of time and isotopic disequilibrium was preserved.

Acknowledgements

We wish to thank Mrs G. Bartholomä who prepared the titanite separates and Mr Ch. Münchberg for help in isotope analyses. Special thanks go to Prof. I. Wendt for providing the error equation for the initial Sr ratio (see

Appendix). Roberta Rudnick (editorial handling) and two anonymous reviewers are thanked for their comments that helped to strengthen the article. **[RLR]**

Appendix A

The following equations outline the derivation of the formula used for calculating the uncertainty of the initial $^{87}Sr/^{86}Sr$ ratio of an individual sample for a given age (t).

In the Rb–Sr decay scheme, the initial $^{87}Sr/^{86}Sr$ ratio can be expressed as follows:

$$\left(\frac{^{87}Sr}{^{86}Sr}\right)_0 = \frac{^{87}Sr}{^{86}Sr} - \frac{^{87}Rb}{^{86}Sr}\left(e^{\lambda t} - 1\right)$$

where $(^{87}Sr/^{86}Sr)_0$ is the initial $^{87}Sr/^{86}Sr$ ratio in the rock or mineral, λ is the ^{87}Rb decay constant and $^{87}Rb/^{86}Sr$ and $^{87}Sr/^{86}Sr$ the present-day measured isotopic ratios.

The error for this equation is given by:

$$\partial\left(\frac{^{87}Sr}{^{86}Sr}\right)_0 = \partial\frac{^{87}Sr}{^{86}Sr} - \left(e^{\lambda t} - 1\right) \times \partial\frac{^{87}Rb}{^{86}Sr} - \frac{^{87}Rb}{^{86}Sr} \times \lambda \times e^{\lambda t} \times \partial t$$

simplification by the approximation $e^{\lambda t} - 1 \approx \lambda t$ yields:

$$\partial\left(\frac{^{87}Sr}{^{86}Sr}\right)_0 = \partial\frac{^{87}Sr}{^{86}Sr} - \lambda t \times \partial\frac{^{87}Rb}{^{86}Sr} - \frac{^{87}Rb}{^{86}Sr} \times \lambda \times e^{\lambda t} \times \partial t.$$

The resulting equation for the error of the initial $^{87}Sr/^{86}Sr$ ratio is:

$$\sigma\left(\frac{^{87}Sr}{^{86}Sr}\right)_0^2 = \sigma\left(\frac{^{87}Sr}{^{86}Sr}\right)^2 + (\lambda t)^2 \times \sigma\left(\frac{^{87}Rb}{^{86}Sr}\right)^2 + \left(\lambda \times \frac{^{87}Rb}{^{86}Sr} \times e^{\lambda t}\right)^2 \times \sigma t^2$$

This equation was used for calculating the error bars of individual samples shown in Fig. 4. The error mainly depends on the first and second term of this equation. The last term, $(\lambda \times {}^{87}Rb/{}^{86}Sr \times e^{\lambda t})^2 \times \sigma t^2$, includes the uncertainty of the assumed age of the host rock. The contribution of this term to the calculated error is generally very small and it can be omitted if $^{87}Sr/^{86}Sr$ ratios from the same mineral or different minerals from the same host rock are compared.

References

Bizzarro, M., Simonetti, A., Stevenson, R.K., Kurszlaikis, S., 2003. In situ $^{87}Sr/^{86}Sr$ investigation of igneous apatites and carbonates using laser-ablation MC-ICP-MS. Geochim. Cosmochim. Acta 67, 289–302.

Brandmayr, M., Dallmeyer, R.D., Handler, R., Wallbrecher, E., 1995. Conjugate shear zones in the southern Bohemian Massif (Austria): implications for Variscan and Alpine tectonothermal activity. Tectonophysics 248, 97–116.

Chen, F., Siebel, W., 2004. Zircon and titanite geochronology of the Fürstenstein granite massif, Bavarian Forest, NW Bohemian Massif: pulses of Late Variscan magmatic activity. Eur. J. Mineral. 16, 777–788.

Cherniak, D.J., 1993. Lead diffusion in titanite and preliminary results on the effects of radiation damage on Pb transport. Chem. Geol. 110, 177–194.

Cherniak, D.J., Watson, E.B., 1992. A study of strontium diffusion in K-feldspar, Na–K feldspar and anorthite using Rutherford backscattering spectroscopy. Earth Planet. Sci. Lett. 113, 411–425.

Cherniak, D.J., Watson, E.B., 1994. A study of strontium diffusion in plagioclase using Rutherford backscattering spectroscopy. Geochim. Cosmochim. Acta 58, 5179–5190.

Cherniak, D.J., Watson, E.B., 2000. Pb diffusion in zircon. Chem. Geol. 172, 5–24.

Christensen, J.N., DePaolo, D.J., 1993. Time scales of large volume silicic magma systems: Sr systematics of phenocrysts and glass from the Bishop Tuff, Long Valley, California. Contrib. Mineral. Petrol. 113, 100–114.

Christensen, J.N., Halliday, A.N., Der-Chuen, L., Hall, C.M., 1995. In situ Sr isotopic analysis by laser ablation. Earth Planet. Sci. Lett. 136, 79–85.

Christinas, P., Köhler, H., Müller-Sohnius, D., 1991. Altersstellung und Genese der Palite des Vorderen Bayerischen Waldes (Nordostbayern). Geol. Bavarica 96, 87–107.

Cox, R.A., Dempster, T.J., Ball, B.R., Rodgers, G., 1996. Crystallization of the Shap granite: evidence from zoned K-feldspar megacrysts. J. Geol. Soc.(London) 153, 625–635.

Davidson, J.P., Tepley III, F.J., 1997. Recharge in volcanic systems; evidence from isotope profiles of phenocrysts. Science 275, 827–829.

Davidson, J.P., Tepley III, F.J., Knesel, K.M., 1998. Isotopic fingerprinting may provide insight into evolution of magmatic systems. EOS 79, 185–193.

Davidson, J.P., Tepley III, F.J., Palacz, Z., Meffan-Main, S., 2001. Magma recharge, contamination and residence times revealed by in situ laser ablation isotopic analysis of feldspar in volcanic rocks. Earth Planet. Sci. Lett. 184, 427–442.

Davies, G.R., Halliday, A.N., Mahood, G.A., Hall, C.M., 1994. Isotopic constraints on the production rates, crystallisation histories and residence times of pre-caldera silicic magmas, Long Valley, California. Earth Planet. Sci. Lett. 125, 17–37.

Deer, W.A., Howie, R.A., Zussman, J., 2001. Rock-forming minerals. Framework Silicates: Feldspars, Geol. Soc. London, Spec. Publ., vol. 4a. 972 pp.

Dodson, M.H., 1973. Closure temperature in cooling geochronological and petrological systems. Contrib. Mineral. Petrol. 40, 259–274.

Feldstein, S.N., Halliday, A.N., Davies, G.R., Hall, C.M., 1994. Isotope and chemical microsampling: constraints on the history of an S-type rhyolite, San Vincenzo, Tuscany, Italy. Geochim. Cosmochim. Acta 58, 943–958.

Frentzel, A., 1911. Das Passauer Granitmassiv. Geognostisches Jahrb. 24 (31 pp).

Frost, B.R., Chamberlain, K.R., Schumacher, J.C., 2000. Sphene (titanite): phase relations and role as a geochronometer. Chem. Geol. 172, 131–148.

Gagnevin, D., Daly, J.S., Waight, T.E., Morgan, D., Poli, G., 2005. Pb isotopic zoning of K-feldspar megacrysts determined by laser ablation multi-collector ICP-MS: insights into granite petrogenesis. Geochim. Cosmochim. Acta 69, 1899–1915.

Geist, D.J., Myers, J.D., Frost, C.D., 1988. Megacryst-bulk rock isotopic disequilibrium as an indicator of contamination processes: the Edgecumbe volcanic field, SE Alaska. Contrib. Mineral. Petrol. 99, 105–112.

Giletti, B.J., 1991. Rb and Sr diffusion in alkali feldspars, with implications for cooling histories of rocks. Geochim. Cosmochim. Acta 55, 1331–1343.

Giletti, B.J., Casserly, J.E.D., 1994. Strontium diffusion kinetics in plagioclase feldspars. Geochim. Cosmochim. Acta 58, 3785–3793.

Halama, R., Waight, T., Markl, G., 2002. Geochemical and isotopic zoning patterns of plagioclase megacrysts in gabbroic dykes from the Gardar Province, South Greenland: implications for crystallisation processes in anorthositic magmas. Contrib. Mineral. Petrol. 144, 109–127.

Horn, P., Köhler, H., Müller-Sohnius, D., 1986. Rb–Sr Isotopengeochemie hydrothermaler Quarze des Bayerischen Pfahls und eines Fluβspat-Schwerspat-Ganges von Nabburg-Wölsendorf/Bundesrepublik Deutschland. Chem. Geol. 58, 259–272.

Jenkin, G.R.T., Rogers, G., Fallick, A.E., Farrow, C.M., 1995. Rb–Sr closure temperatures in bi-mineralic rocks: a mode effect and test for different diffusion models. Chem. Geol. 122, 227–240.

Jenkin, G.R.T., Ellam, R.M., Rogers, G., Stuart, F.M., 2001. An investigation of closure temperature of the biotite Rb–Sr system: the importance of cation exchange. Geochim. Cosmochim. Acta 65, 1141–1160.

Knesel, K.M., Davidson, J.P., Duffield, W.A., 1999. Open-system evolution of silicic magma by assimilation followed by recharge: evidence from Sr isotopes in sanidine phenocrysts, Taylor Creek rhyolite, NM. J. Petrol. 40, 773–786.

Leichmann, J., Broska, I., Zachovalová, K., 2003. Low-grade metamorphic alteration of feldspar minerals: a CL study. Terra Nova 15, 104–108.

Ludwig, K.R., 1993. PBDAT: a computer program for processing Pb–U–Th isotope data, version 1.2, USGS Open-file Report 88–542, 30 pp.

Ludwig, K.R., 2003. Isoplot 3.00—a geochronological toolkit for Microsoft Excel: Berkeley Geochronology Center. Spec. Publ. 4.

Müller, W., 2003. Strengthening the link between geochronology, textures and petrology. Earth Planet. Sci. Lett. 206, 237–251.

Ramos, F.C., Wolff, J.A., Tollstrup, D.L., 2004. Measuring $^{87}Sr/^{86}Sr$ variations in minerals and groundmass from basalts using LA–MC-ICPMS. Chem. Geol. 211, 135–158.

Schmidberger, S.S., Simonetti, A., Francis, D., 2003. Small-scale Sr isotope investigation of clinopyroxenes from peridotite xenoliths by laser ablation MC-ICP-MS — implications for mantle metasomatism. Chem. Geol. 199, 317–329.

Siebel, W., Blaha, U., Chen, F., Rohrmüller, J., 2005. Geochronology and geochemistry of a dyke–host rock association and implications for the formation of the Bavarian Pfahl shear zone, Bohemian Massif. Int. J. Earth Sci. 94, 8–23.

Siebel, W., Thiel, M., Chen, F., in press. Zircon geochronology and compositional record of late-to post-kinematic granitoids associated with the Bavarian Pfahl zone (Bavarian Forest) Mineral. Petrol.

Steiner, L., 1969. Kalifeldspatisierung in den Palitgesteinen des Pfahlgebietes. Geol. Bavarica 60, 163–169.

Steiner, L., 1972. Alkalisierung im Grundgebirge des Bayerischen Waldes. Neues Jahrb. Mineral. Abh. 116, 132–166.

Troll, G., 1964. Das Intrusivgebiet von Fürstenstein (Bayerischer Wald). Geol. Bavarica 52 (140 pp.).

Troll, G., 1967. Die blastokataklastischen Kristallingesteine der Stallwanger Furche, Bayerischer Wald. Geol. Bavarica 58, 22–33.

Waight, T.E., Dean, A.A., Maas, R., Nicholls, I.A., 2000a. Sr and Nd isotopic investigations towards the origin of feldspar megacrysts in microgranular enclaves in two I-type plutons of the Lachlan Fold Belt, southeast Australia. Aust. J. Earth Sci. 47, 1105–1112.

Waight, T.E., Maas, R., Nicholls, I.A., 2000b. Fingerprinting feldspar phenocrysts using crystal isotopic composition stratigraphy: implications for crystal transfer and magma mingling in S-type granites. Contrib. Mineral. Petrol. 139, 227–239.

Waight, T.E., Baker, J.A., Peate, D.W., 2002. Sr isotope ratio measurements with a double-focussing MC-ICPMS: techniques, observations and pitfalls. Int. J. Mass Spectrom. 221, 229–244.

Wendt, I., 1986. Radiometrische Methoden in der Geochronologie. Clausthal. Tekton. Hefte 23, 1–170.